INTERNATIONAL JOURNAL OF AUTOMOTIVE AND MECHANICAL ENGINEERING
ISSN: 2229-8649 e-ISSN: 2180-1606
VOLUME 23, ISSUE 2, 2026, 13554 - 13567
DOI: https://doi.org/10.15282/ijame.23.2.2026.7.1026

RESEARCH ARTICLE

Effect of die orientation on the mechanical and physical properties of 356 aluminium alloy castings produced by gravity die casting

Saleh Suliman Saleh Elfallah[1]*, and Mohd Radzi Mohamed Yunus[2]

[1]College of Mechanical Engineering Technology, Benghazi, Libya
[2]Faculty of Mechanical and Manufacturing Engineering, Universiti Tun Hussein Onn Malaysia, Parit Raja 86400, Malaysia

Abstract - Al–Si–Mg alloys are widely used in automotive and aerospace applications due to their excellent castability and mechanical properties. Gravity die casting (GDC) is commonly employed to manufacture such components. While AISI H13 tool steel is typically preferred for GDC dies, mild steel dies may be used for low-volume production because of their lower cost and ease of fabrication. However, mild steel dies generally exhibit limited-service life due to lower hardness, reduced wear resistance, and poor thermal fatigue resistance. Therefore, optimisation of casting parameters is necessary to improve casting quality. This study evaluates the influence of die orientation and pouring temperature on the mechanical, physical, microhardness, and porosity characteristics of aluminium (Al) alloy 356 castings produced using an ASTM A36 mild steel gravity die. The casting process was conducted at different pouring temperatures using vertically oriented casting (VOC) and horizontally oriented casting (HOC) configurations. The resulting castings were evaluated through impact testing, microhardness measurements, and porosity analysis, including apparent porosity (AP) and bulk porosity (BP). Results show that VOC at a pouring temperature of 900 °C improved impact toughness by 59.3% (average 16 kJ/m^2) compared with HOC, while reducing surface microhardness by 2.4% (82.7 HV). Additionally, VOC significantly reduced BP by 91.9% and AP by 69.5%. Compared with castings produced at 800 °C, VOC at 900 °C increased impact toughness by 34.3% and reduced BP by 75.15%. Overall, vertically oriented casting using mild steel dies significantly improves impact toughness and reduces porosity in 356 Al alloy castings.

Article History
Received : 11 October 2025
Revised : 5 March 2026
Accepted : 29 April 2026
Published : 30 June 2026

Keywords
Aluminium casting
Mild steel die
Gravity die casting
Mechanical properties
Porosity

1. Introduction

Aluminium (Al) alloys are widely utilised in various engineering applications such as automotive and aerospace parts. Al is increasingly replacing steel components in automotive systems and engines due to its lower weight, which is essential for improving fuel efficiency and reducing harmful emissions and overall engine performance [1,2]. However, casting defects such as porosity, inclusions, and irregular microstructures are obstacles to achieving maximum strength [3]. Continuous efforts have focused on improving casting quality and optimising processing parameters to enhance the mechanical reliability of Al cast products [4].

Al alloys castings are widely used for their superior lubricity, superior corrosion resistance, and favourable mechanical properties [5]. Among aluminium casting alloys, Al-Si-Mg alloys have excellent castability, high specific strength and excellent corrosion resistance and are therefore suitable for the production of thin-walled automotive structural parts by means of the high-pressure die casting (HPDC) process [6] and gravity die casting (GDC) [7]. Al-Si-Mg alloys can be optimised to achieve a wide range of mechanical properties, which make them suitable for a variety of automotive applications [5]. The silicon (Si) content of these alloys may be adjusted according to the specific casting processes and the thickness of the shell. In cases of higher cooling temperatures or thinner mould edges, increasing the Si content may promote better dissolution. In addition, Mg in Al alloys, as seen in Al-Mg alloys, increases their resistance to cracking [8]. Furthermore, the mechanical properties of Al-Si-Mg depend on the degree of Mg_2Si substitution in the Al matrix, the shape and distribution of the Si-phase and the size of the Fe compounds [5]. The microstructure of these alloys usually consists of an Al matrix reinforced with Si and Mg_2Si, together with Si particulates and iron (Fe)-rich intermetallic compounds, which play a crucial role in determining the strength, ductility, and fracture behaviour of the alloy [8]. Therefore, controlling the solidification conditions during casting is essential to achieve favourable microstructural characteristics and improved mechanical performance.

Gravity die casting (GDC) is one of the most widely used manufacturing processes for producing aluminium alloy components with relatively complex geometries and good surface finish [9]. The process of GDC involves filling a mould with melt as a result of gravity. It can be poured into metal or sand moulds. The automotive industry primarily uses gravity casting for light alloy components like wheel discs and cylinder heads [10]. Temperature control is one of the most important factors that determines the success of GDC. In particular, the die and core temperatures have a significant impact on the final mechanical properties and microstructure of the cast Al. The die temperature, which represents the thermal environment of the mould, and the core temperature, which represents the interior of the casting. Changes in these temperatures may have an impact on the Al alloy's grain structure, rate of solidification, and phase formation. They thus have a direct effect on the cast component’s mechanical characteristics, such as its tensile strength, hardness, and ductility.

*CORRESPONDING AUTHOR | S.S.S. Elfallah | ✉ sselfallah87@gmail.com

Recent studies have explored the effects of pouring temperature and melt overheating on the microstructure and mechanical properties of Al-Si-Mg alloys. Deev et al. [11] studied the effect of melt overheating on the mechanical properties and microstructure of AA 511 Al alloy using GDC and reported that higher pouring temperatures (900 °C) improved tensile strength that reached a maximum of 228 MPa and hardness that showed a maximum of 56.5 HV due to grain refinement and reduced dendritic structures that decreased from 39.12 µm of the as-received alloy to 13.01 µm. Similarly, other studies on 356 Al alloy castings have indicated that pouring temperatures reaching 800 °C yield superior mechanical and microstructural outcomes, showing a coarser α-Al dendritic structure [12], [13]. Doty et al. [13], on the performance of the 356 Al alloy, a cylinder head cast at a pouring temperature of 800 °C, found that pouring at 800 °C resulted in an increased hardness of more than 85 BHN and a tensile strength of more than 280 MPa. More recent investigations have also confirmed that melt temperature significantly affects dendrite arm spacing, porosity formation, and phase distribution in Al-Si casting alloys, which directly influence the strength and reliability of cast components [14].

In addition to conventional mechanical properties such as tensile strength and hardness, impact toughness is an important parameter for evaluating the performance of cast components subjected to dynamic or impact loading conditions. Unlike tensile properties, relatively fewer studies have examined the relationship between pouring temperature and impact toughness in Al alloy castings. Previous research has shown that increasing pouring temperature may improve impact resistance by modifying the microstructure and reducing casting defects. For instance, Akhyar et al. [15] reported that increasing the pouring temperature to 788°C in GDC of the AA-2024 alloy improved both hardness (maximum 103 BHN) and impact toughness (maximum 7.48 kJ/m^2). Similar observations were reported by Syahid et al. [16] and Rajaravi et al. [17], who demonstrated that higher processing temperatures (760 °C and 820 °C, respectively) can influence fracture behaviour and toughness characteristics in Al alloy castings of Al alloy AA6061 and Al alloy A356 MMC, respectively. Moreover, a study by Patel et al. [18] investigated the effect of processing temperature on AA2024 MMC by stir casting and found that processing temperature improves the hardness and impact toughness of the stir-cast composite. Nevertheless, these investigations mainly focused on pouring temperature effects under conventional casting configurations.

Among the casting factors, an important but less explored factor influencing casting quality is the orientation of the mould cavity during solidification. The die orientation can affect the melt flow behaviour, solidification patterns, and the distribution of shrinkage porosity, consequently affecting the final microstructure and mechanical properties of cast components. Recent studies suggested that mould casting orientation or cavity design configuration may influence feeding behaviour, defect formation, and thermal gradients within the cavities [19], [20]. However, most existing studies have primarily examined pouring temperature or alloy composition independently, and limited attention has been given to the effect of pouring temperature and die orientation on the mechanical and physical properties of Al alloy castings. It is of importance to understand how pouring temperature interacts with die orientation to influence mechanical and microstructure characteristics for improving casting design strategies and optimising mould design for enhanced mechanical performance.

This study contributes to Al casting research by investigating the mechanical and physical properties of 356 Al alloy castings produced by the GDC technique in a mild steel ASTM A36 permanent mould. The study examines on studying the impact toughness, surface microhardness, and porosity of castings arranged in vertical and horizontal orientations at varying melt overheating temperatures. The pouring temperature effect on the mechanical properties and physical characteristics was evaluated.

1.1 Sub-Section Headings

Section headings must be numbered consecutively using Arabic numerals, starting with the Introduction as Section 1. All primary headings should be left-aligned, formatted in the IJAME Heading 1 style, and capitalised in title case. Secondary headings (second level) should be numbered with two digits (e.g., 2.1, 2.2), formatted in the IJAME Heading 2 style, with the first letter capitalised (title case). Tertiary headings (third level) are numbered with three digits (e.g., 2.1.1), formatted in sentence case, and italicised. Avoid headings beyond the third level whenever possible.

2. Materials and Methods

The permanent mould was fabricated from ASTM A36 mild steel [21], while the casting material, 356 Al alloy, conforming to the specifications of ASTM B108/B108M [22]. Their chemical compositions are presented in Table 1, while their mechanical properties are provided in Table 2. The Brinell hardness (HB) and impact toughness values for the 356 Al alloy were obtained from fr Bahador et al. [23] as listed in Table 2.

Table 1. The chemical compositions of the ASTM A36 mild steel and 356 Al alloy

Component	Material	Elements (wt.%)											
		Al	Si	Mg	Zn	Mn	Fe	Cu	Other	C	P	S	Ti
Mould	Mild steel	-	< 0.04	-	-	0.60-0.90	Balance	0.20	-	0.29	0.04	0.05	-
Casting	AA 356	Balance	6.50-7.50	0.20-0.45	0.35	0.35	0.60	0.25	< 0.20	-	-	-	0.25

Table 2. The tensile properties and hardness of the ASTM A36 mild steel and 356 Al alloy

Component	Material	Tensile properties			Brinell hardness (HB)	Impact toughness (kJ/m^2)
		Yield strength (N/mm^2)	Tensile strength (N/mm^2)	Elongation (%)		
Mould	Mild steel	250	400-500	20 in 200 mm	119-162	Charpy V-notch (27)
Casting	AA 356	69	145	3	27	58

The mould design was developed in consultation with casting specialists. The ratio for the gating system sprue, runner, and ingates is 1:1:2, respectively, as shown in Figures 1 and 2. The gating system follows an established unpressurised gating ratio for conventional casting. The cross-sectional areas of the gating system control melt flow and turbulence during the pouring process, as described by Campbell [24]. The figures illustrate a schematic of the vertical orientation (Figure 1) and horizontal orientation (Figure 2), showing the sprue and runner, each with a diameter of 20 mm, and each of the four ingates with a diameter of 10 mm.

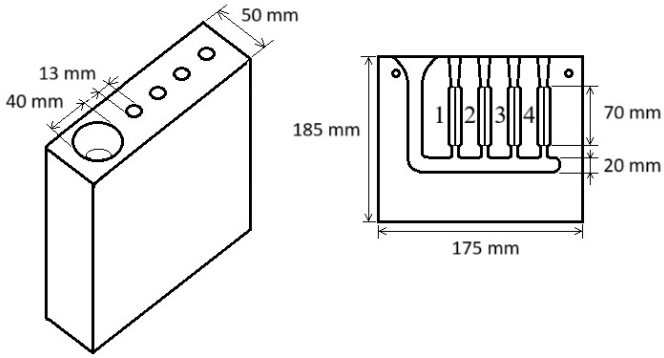

Figure 1. GDC sketch design showing vertical orientation

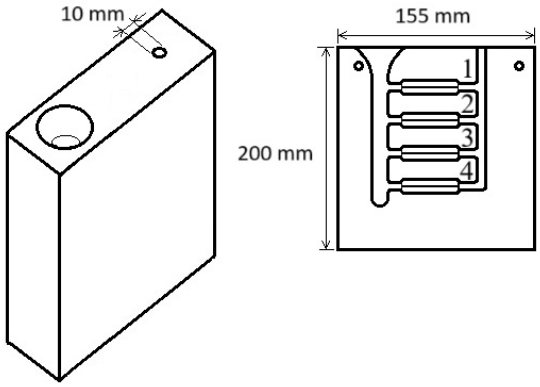

Figure 2. GDC sketch design showing horizontal orientation

The SolidWorks® design layout of the gravity die casting (GDC) mould is presented in Figure 3, which illustrates half of each mould assembly. Figure 3a depicts the horizontally oriented mould, while Figure 3b illustrates the vertically oriented mould. The cavities are connected to a central runner system fed by a top-located sprue cup, which directs the molten metal uniformly into each cavity. The final machined GDC moulds are presented in Figure 4.

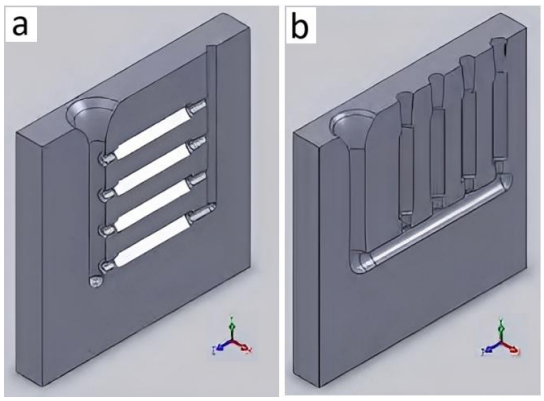

Figure 3. Solidworks® design layout of the GDC showing (a) horizontal orientation, and (b) vertical orientation

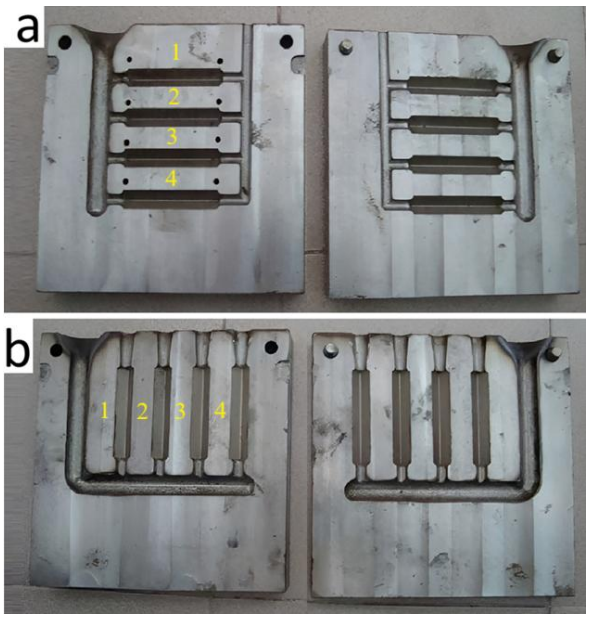

Figure 4. Final machined GDC mould showing (a) horizontal orientation, and (b) vertical orientation

The positions were designed according to ASTM E23 for the Izod impact test as shown in Figure 5, while the multi-cavity mould layout and gating configuration were developed following the design methodology proposed by Kumar et al. [25]. The guidelines provide recommendations for determining cavity arrangement and integrating the gating system in multi-position die casting dies, however, in the present study, the same gating geometry maintained for both vertically oriented casting (VOC) and horizontally oriented casting (HOC) configurations to ensure that the observed casting properties were primarily influenced by mould orientation rather than variations in the gating system. The permanent mould was fabricated by machining ASTM A36 hot-rolled mild steel flat bar stock measuring 175 mm × 185 mm × 50 mm for vertical orientation and 200 mm × 155 mm × 50 mm for horizontal orientation. Each mould block was sectioned in half, and each inner face was face milled to achieve a flat and uniform parting surface. This was followed by rough pocketing and a finishing pass, including rib and channel machining, and corner finishing using multiple end mill tools. All machining processes were carried out in the Computer Numerical Control (CNC) laboratory at Universiti Tun Hussein Onn Malaysia (UTHM). The 356 Al alloy ingots used in this study were sourced from TRIM Industries, Selangor.

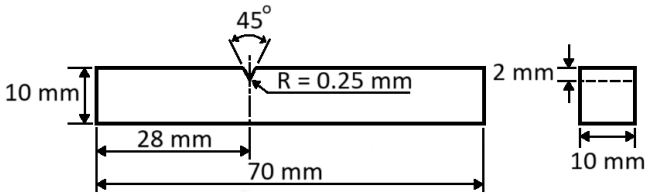

Figure 5. Izod impact test specimen prepared according to ASTM E23

The moulds, prior to pouring, were sprayed with silicone, clamped closed, and preheated using a gas torch to 150 °C, as illustrated in Figure 6, which shows the pouring process at 900 °C. A study by Pratikno et al. [26] on welding A36/A53 joints using FCAW reported that preheating to 150 °C enhanced tensile strength and improved the microstructure. Mould heating required between 10 and 15 minutes using two torches, each heating one side of the mould at the centre to allow heat to distribute evenly. The mould and molten aluminium temperatures were measured using a digital probe thermometer. To maintain the mould preheating temperature, the torches were turned off as soon as the temperature approached 150 °C inside the mould and turned on again prior to and during the pouring process. After pouring, preheating was immediately ceased to allow the mould and casting to cool to room temperature. The pouring height was maintained between 5 and 7 cm above the pouring basin, as shown in Figure 6. Preheating improves casting quality by ensuring smoother melt flow and preventing premature freezing of the Al alloy during pouring. Furthermore, it influences the solidification behaviour of the alloy by controlling the cooling rate, which improves microstructural uniformity, affects dendritic arm spacing, and affects phase distribution in Al alloy castings [27]. In addition, a controlled cooling rate reduces casting defects such as porosity [28]. However, according to the Structural Welding Code-Steel [29], the minimum recommended preheating temperature for welding A36 is 65°C for thicknesses above 38 mm and below 65 mm [29].
Trial pours were initially carried out starting from 700 °C, since alloy 356 has a liquidus temperature of approximately 615 °C. It was determined that 800 °C was the minimum pouring temperature sufficient to completely fill all positions. Consequently, three pouring temperatures were selected: 800, 850, and 900 °C. It is worth noting that higher pouring temperatures, while improving filling, tend to cause long-term damage to the mould.

The Izod impact test was conducted in accordance with ASTM E23 using a Wolpert impact tester. Test specimens were prepared as illustrated in Figure 5, with each reading corresponding to a single sample. Porosity was measured by applying Archimedes' principle using a Mettler Toledo XS64 density tester on specimens with dimensions of 10 mm × 10 mm × 10 mm. Vickers microhardness testing was performed using a Shimadzu HMV-2T with a 0.3 kgf load and a 10 s dwell time on the surface of the castings. Porosity results represent the average of two readings, while microhardness values were averaged over three readings. The evaluation of casting macro-porosity was performed through visual inspection, categorising the porosity density into low, moderate, and high, whereby the cross-sections of the samples were captured using a high-resolution camera. The samples were sectioned from the middle of the castings, as schematically illustrated in Figure 7. The cross-sectional surfaces were then ground using sandpaper up to 1200 grit and subsequently polished with alumina to obtain a smooth surface that clearly revealed the porosity along the casting cross-sections.

Figure 6. Pouring process at 900 °C for the vertical orientation mould

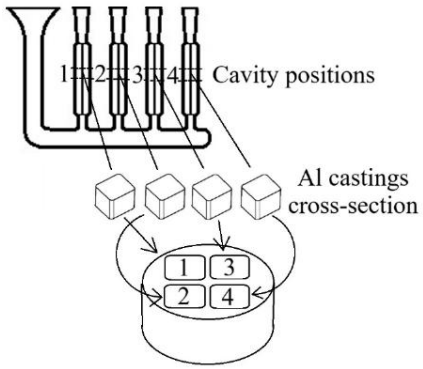

Figure 7. Schematic illustration showing the cross-sectional locations of macro-porosity samples extracted from the middle cavity positions of VOC

3. Results and Discussion

The pouring time for each trial was measured using a stopwatch, and the results are presented in Table 3. Pouring time is a critical process parameter that characterises the melt flow behaviour under each mould orientation.

Table 3. The pouring time in second counted manually for each mould orientation

	Horizontal orientation mould	Vertical orientation mould
Pouring temperature (°C)	Time (s)	Time (s)
800	2.20	2.40
850	2.06	2.72
900	1.92	2.05

It is noticed from Table 3 that the vertical orientation mould is filled slower than horizontal orientation. This is due to it has lower volume capacity 77.9 cm^3 compared to 94.2 cm^3 for vertical orientation. The casting mass for vertical orientation mould (252.4 g) and horizontal orientation mould (208.7 g) were calculated knowing the density of 356 Al alloy density is 2.68 g/cm^3. The pouring time (t_p) depends on the volume of the position, sprue cross-sectional area, and metallostatic head [24]. It can be calculated using the classic Torricelli's theorem (Equation 1):

$$t_p = \frac{V}{C_d A\sqrt{2gh}} \quad (1)$$

where V is the mould position volume (cm^3), A the sprue cross-sectional area (cm^2), h the metallostatic head (cm), g is 981cm/s^2, and C_d (0.6 for harp turns with multiple positions and higher turbulence) accounts for gating losses and turbulence [24], [30]. Table 4 show the calculated t based on Torricelli's theorem, the theoretical exit velocity (v) (Equation 2) and flow rate (Q) (Equation 3). The theoretical time calculated using Torricelli's theorem was significantly higher than the manually measured values in Table 3, indicating that Torricelli's theorem does not accurately represent the pouring time for 356 Al alloy casting.

Table 4. The theoretical pouring time, exit velocity and flow rate for each mould orientation

	Vertical orientation mould	Horizontal orientation mould
t_p (s)	0.46	0.38
v (cm/s)	54.25	
Q (cm^3/s)	681.4	

$$v = \sqrt{2gh} \tag{2}$$

$$Q = Av \tag{3}$$

Futas et al. [31] developed a mathematical model for calculating solidification time (t_s) (Equation 4) in sand-clay mould castings, incorporating thermophysical properties and interface heat transfer effects.

$$t_s = b\sqrt{w} \tag{4}$$

where b is the average thickness of the casting walls (cm) and W is weight of crude casting (kg). The casting time for vertical oriented casting (VOC) according to Equation 4 was 0.979 s and 0.89 s for horizontal orientated casting (HOC). The casting time for vertical orientation is higher than horizontal, which is logic due to the casting being larger. In general, the theoretical casting time is more than 0.5 s (about 53 % more for VOC and 57 % for HOC), greater than the theoretical pouring time, as shown in Table 4. However, the theoretical cast time is also lower than the calculated manual pouring time (Table 3). Futas et al. [31] have also proposed incorporating gate geometry cross-section formula for ductile iron (C_A). The formula as shown in Equation 5 determines the cross section at the bottom of the sprue.

$$C_A = \frac{22.6 \times W}{\delta \times \xi \times t_s \times \sqrt{H}} \tag{5}$$

where δ is cast density (g/cm^3), ξ is the friction factor 0.47 for sliding solid Al on solid mild steel [33], and H is effective pouring height (cm) as shown in Equation 6.

$$H = \frac{P^2}{2C} \tag{6}$$

where h is the height difference between the melt level in the pouring basin and the centre of the ingates (cm), P is the height of the casting above the ingate (cm), and C is the height of the casting in the mould (cm). The resultant metallostatic head H is approximately 11.71 cm for the vertical orientation mould (with h = 12 cm, P = 2 cm and C = 7 cm) and about 10 cm for the horizontal orientation mould (with h = 10 cm, P = 0 cm and C = 14.14 cm). Which is considered higher that the pouring height of the experiments as mentioned earlier. By calculation, the sprue cross-sectional area (C_A) is 1.351 cm² for the vertical orientation mould and 1.33 cm² for the horizontal orientation mould, corresponding to minimum required sprue diameters of 1.31 cm and 1.30 cm, respectively. In comparison, the sprue and runner diametersused in this study were 2 cm each, as seen in Figure 1 and Figure 2, which is more than sufficient. According to Futas et al. [31], the gating system should always expand toward the casting by at least 10%. However, in the present moulds used for experimentation, the sprue and runner areas in both vertical and horizontal orientations are each 3.14 cm², with a combined ingate area of 3.14 cm². Meaning the ratio is constant as indicated in the Materials and Methods section. Therefore, the mould designs ratios employed in this study do not follow the cited recommendation.

The final castings are shown in Figures 8 and 9 for VOC and HOC, respectively. The results indicate that higher pouring temperatures lead to more side flash on the castings, particularly in HOC. This effect can be attributed to the increased fluidity of the molten Al and the greater thermal expansion within the mould, which tends to force open the mould parting line at narrow sections. The casting surfaces exhibited minor defects such as pinholes, misruns, and cold shuts. Furthermore, the enhanced fluidity of molten Al at elevated pouring temperatures increases its ability to adequately reach the distant cavity positions and their outlets, as seen in Figures 8(c) and 9(c). In addition, increased fluidity was reported to reduce shrinkage porosity and ensure complete mould filling [32]. Nevertheless, elevated pouring temperature accelerated mould wear, which necessitates mould replacement after a number of casting cycles.

Figure 8. Final HOC at pouring temperatures (a) 800 °C, (b) 850 °C and (c) 900 °C for the horizontal orientation mould

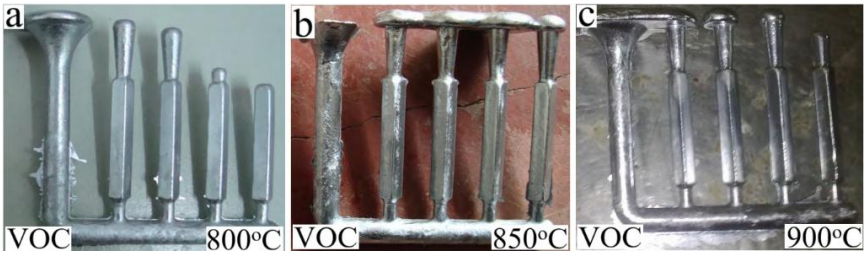

Figure 9. Final VOC at pouring temperatures (a) 800 °C, (b) 850 °C and (c) 900 °C for the vertical orientation mould

The Izod impact toughness results for VOC and HOC are shown in Table 5. Further details of these results are illustrated in Figures 10(a) and 10(b). Figure 10(a) presents the impact toughness at each pouring temperature, while Figure 10(b) shows the average impact toughness at each cavity position. The results indicate a maximum impact toughness of 19 kJ/m² recorded at both 800 °C and 900 °C pouring temperatures, achieved by VOC.

Table 5. The impact toughness for VOC and HOC

Pouring temperature	Cavity position	VOC (kJ/m^2)	HOC (kJ/m^2)
800 °C	1	6	4
	2	9	19
	3	19	6
	4	8	4
850 °C	1	6	4
	2	14	4
	3	10	4
	4	6	3
900 °C	1	13	2
	2	16	6
	3	19	11
	4	16	7

Figures 10(a) and 10(b) clearly demonstrate that VOC exhibited impact toughness averages more than 54% higher than HOC. Furthermore, impact toughness increased with pouring temperature, reaching its highest value at 900 °C, as seen in Figure 10(a). The highest impact toughness was also observed at the middle cavity positions 2 and 3, with the highest value of 16 kJ/m² recorded at position 3 of VOC, as shown in Figure 10(b).

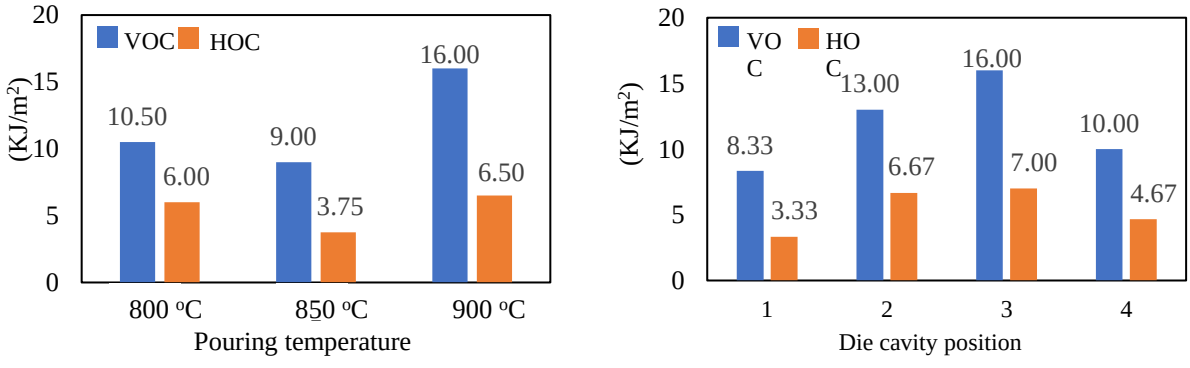

Figure 10. The Averages for impact toughness of castings; (a) At different pouring temperatures, (b) At each cavity position

The Vickers microhardness results for VOC and HOC are shown in Table 6, while Figures 11(a) and 11(b) illustrate the microhardness at each pouring temperature and at each cavity position, respectively. The results indicate a maximum hardness of 115 HV at 850 °C. Figures 11(a) and 11(b) show that VOC exhibited a slightly higher average hardness of approximately 6% compared with HOC across all pouring temperatures except 900 °C, where VOC microhardness decreased by 18% compared with 800 °C. The microhardness values across cavity positions showed close agreement, with clearer uniformity observed more clearly in HOC. For HOC, the lowest microhardness of 88.87 HV was recorded at cavity position 2, and the highest of 91.63 HV at position 3. For VOC, position 2 showed the lowest hardness (90.6 HV), and the highest hardness of 101.7 HV was recorded at position 4, as seen in Figure 11(b).

Table 6. The Vickers microhardness for VOC and HOC

Pouring temperature (°C)	Cavity position	VOC (VHN)	HOC (VHN)
800	1	102	94.9
	2	101	98.8
	3	102	101
	4	101	91.3
850	1	108	86.5
	2	88	80
	3	104	94.8
	4	115	93.5
900	1	78.9	87.5
	2	82.8	87.8
	3	79.8	79.1
	4	89.3	85.1

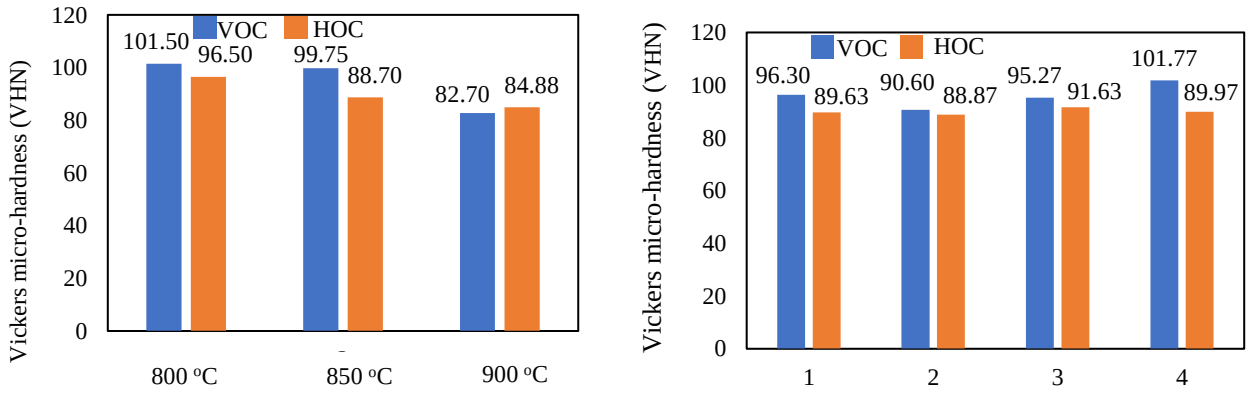

Figure 11. The Averages for impact toughness of castings; (a) At each pouring temperature, (b) At each cavity position

The macro-porosity of the VOC and HOC are shown in Figure 12 and Figure 13 respectively, while Table 7 show the observation evaluation for each cavity position with respect to pouring temperatures. The L denotes to low pouring density, M to moderate, and H to high. Table 8 lists the apparent porosity (AP) and bulk porosity (BP). The first refers the percentage of open pores, while the second refers to the total pore volume for VOC and HOC. The calculations for AP ($(AP(\%))$ and BP ($BP(\%)$) scaled in percentages are presented in Equation 7 and Equation 8 respectively.

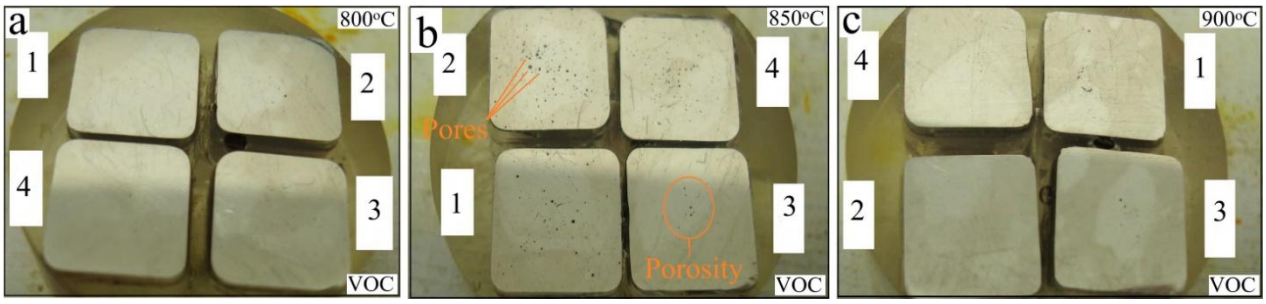

Figure 12. Visual inspection macro-porosity at the cross-section of VOC castings at different pouring temperatures; (a) at 800 °C, (b) at 850 °C, and (c) at 900 °C

Figure 13. Visual inspection of macro-porosity at the cross-section of HOC castings at different pouring temperatures; (a) at 800 °C, (b) at 850 °C, and (c) at 900 °C

Table 7. Macro-porosity characteristics for samples produced at VOC and HOC with respect to pouring temperatures

Pouring temperature	Macro-porosity condition for VOC					Macro-porosity condition for HOC				
	Overall	Cavity position				Overall	Cavity position			
		1	2	3	4		1	2	3	4
800°C	M/L	M	M	L	L	M	H	M	M	M
850°C	H	H	H	M	H	H	H	H	H	H
900°C	M	M	L	M	M	M/H	M	M	H	H

Table 8. The AP and BP for VOC and HOC

Pouring temperature	Cavity position	VOC		HOC	
		Apparent porosity (%)	Bulk porosity (%)	Apparent porosity (%)	Bulk porosity (%)
800°C	1	0.03	26.34	0.29	2.44
	2	0.17	11.53	0.16	18.21
	3	0.46	5.46	5.45	11.98
	4	0.60	8.83	5.42	12.03
850°C	1	0.17	0.96	0.29	0.12
	2	0.19	0.08	0.34	11.93
	3	4.25	9.94	15.91	7.27
	4	4.31	9.95	16.04	7.31
900°C	1	2.24	4.33	0.08	6.52
	2	0.22	3.99	0.07	14.62
	3	0.04	0.39	15.48	10.67
	4	0.01	4.25	15.39	10.68

$$AP(\%) = \frac{W_{wet} - W_{dry}}{W_{wet} - W_{suspended}} \times 100 \quad (7)$$

$$BP(\%) = (1 - \frac{\rho_{bulk}}{\rho_{theoritical}}) \times 100 \quad (8)$$

where W is the weight of the casting, $\rho_{theoritical}$ is the density of 356 Al alloy of 2.68 g/cm^3 and ρ_{bulk} is the dry weight divided by the volume of the sample. Based on the visual inspection evaluation observed in Figures 14 and 15 and listed in Table 7, VOC exhibited lower macro-porosity than HOC. The VOC samples at a pouring temperature of 800 °C have the least macro-porosity of all, showing moderate (M) porosity adjacent to the gating system positions (positions 1 and 2), while the porosity density was low (L) at distant positions. In addition, the VOC porosity increased with increasing pouring temperature, showing high (H) at 850 °C, while it decreased to M at 900 °C. Similarly, the HOC samples exhibited increments in macro-porosity with increasing pouring temperature, reaching a maximum at 850 °C, as seen in Figure 13 and Table 7; however, the HOC samples' macro-porosity was higher than that of VOC samples, showing no categorised L porosity. Moreover, Figure 13 shows large pores, such as those observed in cavity position 1 (Figure 13a), and the pores increased with increasing temperature.

Figure 14(a) shows the average AP of the castings at each pouring temperature. A clear difference is observed between VOC and HOC, with HOC exhibiting more than 83% higher AP, while the BP was higher by more than 24%. This indicates that HOC has much higher open porosity, especially at elevated pouring temperatures of 850 °C and 900 °C, and at the distant positions (positions 3 and 4) as seen in Figure 14(c). Similarly, horizontal castings exhibited higher BP at elevated pouring temperatures (850 °C and 900 °C). However, at 800 °C, VOC showed higher BP, as illustrated in Figure 14(b). Furthermore, as shown in Figure 14(d), HOC exhibited higher distant BP, particularly at positions 2, 3, and

4, which follows the same trend as the AP in Figure 14(c). Overall, VOC produced castings with significantly lower AP. VOC exhibited higher BP at 800 °C, which decreased as the pouring temperature increased. In addition, VOC showed relatively uniform porosity across all positions, with a relatively uniform distribution across all cavity positions.

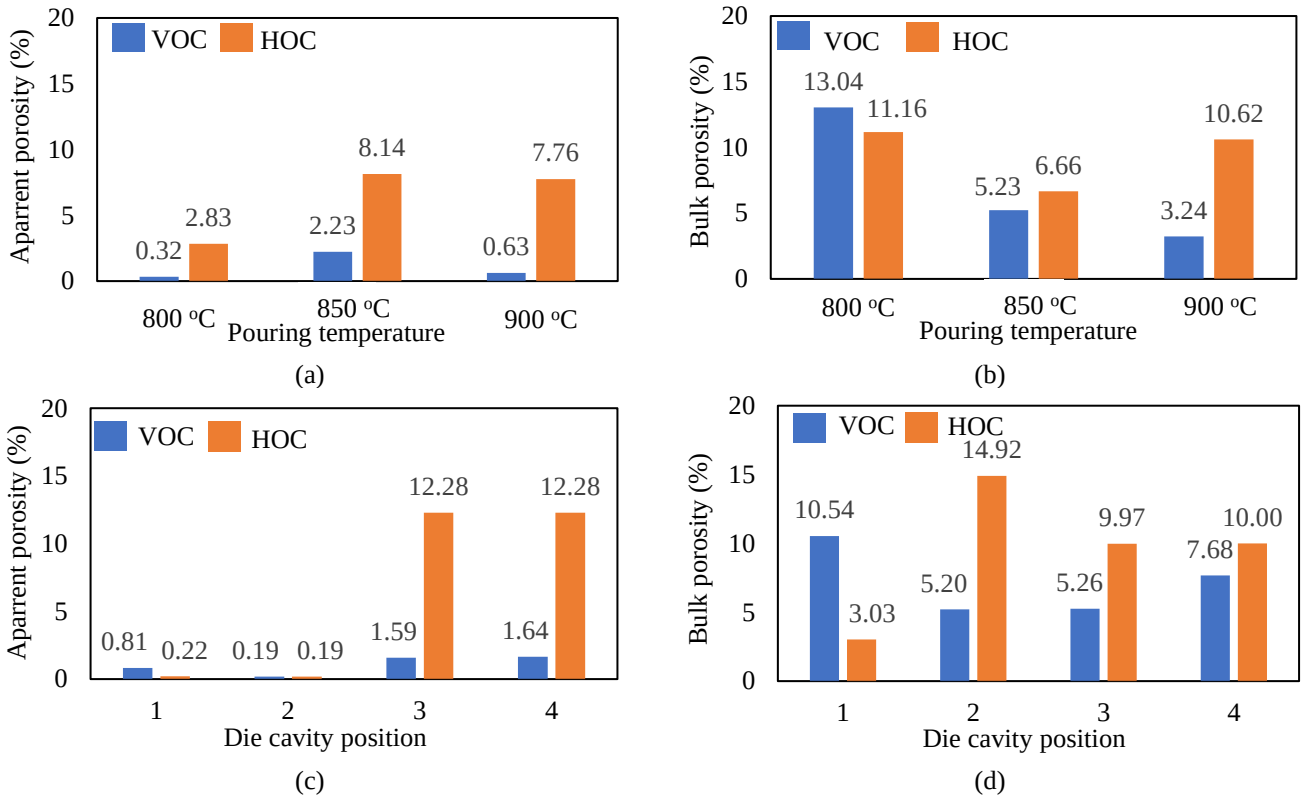

Figure 14. The Averages for AP and BP of the casting; (a) AP at each pouring temperature, (b) BP at each pouring temperature, (c) AP at each cavity position, (d) BP at each cavity position

The cross-sectional macro-porosity for VOC and HOC, as shown in Figures 12, 13, and Table 7, demonstrates a clear pattern with AP in Figure 14(a) with respect to the pouring temperature. The AP shows total agreement with the macro-porosity at all pouring temperatures, where the increased AP at HOC from 2.83% at 800 °C to 8.14% at 850 °C to the slightly decreased 7.76% at 900 °C agrees with the transition in porosity from M to H to M/H. The BP observed increased porosity for HOC (Figure 14(b)) only at elevated pouring temperatures, where the porosity showed H (6.66%) at 850 °C and M/H (10.62%) at 900 °C as interpreted in Table 7. The VOC furthermore showed agreement between the AP, as seen in Figure 14(a), and the increase in porosity at 850 °C, followed by a decrease at 900 °C, as shown in Figure 13 and noted in Table 7. Nevertheless, a contradiction was noticed between the BP and macro-porosity in Figure 13, where the BP was higher for VOC at 800 °C than HOC and decreased with increased pouring temperature. This is unlike the lower macro-porosity for VOC indicated in Figure 12 and Table 7. As per cavity position, the increased per cavity position casting porosity, as observed in distant positions for AP in Figure 14(c) and BP in Figure 14(d), agrees with the macro-porosity index in Table 7, showing M and mostly H. Furthermore, the increased AP and BP for HOC agree with the large pores observed in Figure 13, especially at lower pouring temperatures, such as cavity position 1 at 800 °C in Figure 13(a) and at 850 °C in Figure 13(b). Moreover, the macro-porosity in HOC is sided, as seen clearly in Figure 13(b) at 850 °C, which indicates the descending of porosity upward due to the nature of the horizontal cavity position.

In general, the castings exhibited considerable porosity, with maximum BP values reaching 26.34% at HOC and 18.21% at VOC. Nonetheless, VOC showed approximately 24% lower BP than HOC. The formation of porosity can be attributed to multiple interacting causes during solidification. Samuel et al. [28] reported that solidification shrinkage occurs during the transition of molten Al from liquid to solid, resulting in porosity formation. They also noted that porosity increases due to pressure drops within the solidifying metal caused by volume contraction and insufficient feeding of molten Al. In addition, longer solidification times, especially toward the mould centre, promote porosity development [28]. Other sources of porosity include dissolved gases, primarily hydrogen [28], and entrapped air caused by turbulence [34].

The reason for the decline in BP with increasing pouring temperature remains unclear and warrants further investigation. Furthermore, the higher BP in VOC at 800 °C as seen in Figure 14(b) is anomalous, since the macro-porosity in Figure 12 and Table 7 indicates otherwise. Moreover, it has been reported that increased solidification time due to increased pouring temperature causes increased porosity in the casting [28]. Nevertheless, overall, the lower BP in VOC than HOC could be attributed to the vertical mould configuration, which had open outlets or risers for each cavity position. These outlets improve feeding, reduce entrapped gases [28], reduce solidification time [36], and may cause less flow disturbance in the casting for VOC compared to HOC. In addition, VOC benefits from gravity-assisted downward

flow and compaction of the molten metal, which promotes better densification. Nevertheless, in the VOC design, each position is supplied by its own outlet or riser. This effect is clearly illustrated in Figure 9, where the distant positions (3 and 4) of the VOC show incomplete feeding at lower pouring temperatures, such as 800 °C (Figure 9a); this could be related to the increased AP and BP, especially in position 3 (average AP of 1.59% and BP of 5.26%) and position 4 (average AP of 1.64% and BP of 7.68%), as seen in Figures 14(c) and 14(d).

On the other hand, in the HOC, all positions are connected to a single outlet, which provides more balanced feeding, as shown in Figure 8. However, since the cavities are not directly connected to the riser as in the vertical mould, the casting is more likely to trap porosity. This is seen more clearly in HOC in Figure 13(b), where the macro-porosity takes sides at the cross-sections as discussed earlier. Furthermore, the higher AP, BP, and macro-porosity observed in the HOC, especially at distant positions and under elevated pouring temperatures, is likely related to the longer solidification time. Position 3, with an AP average of 12.28% and a BP of 9.97%, and position 4, with an AP average of 12.28% and a BP of 10.00%, have higher porosity, probably because they are located near the mould centre with no direct connection to the riser or mould surface. Furthermore, the increased pouring temperature (850 °C and 900 °C) caused a longer solidification time for the molten Al [28].

The turbulence of the molten Al during the pouring process is possibly one of the causes of increased porosity in HOC, more likely because the cavity positions connect directly to the sprue, unlike the VOC, where the molten Al passes through the runner and rises to the cavities, mitigating turbulence during flow. It has been reported that higher turbulence in molten Al leads to increased porosity [37]. Furthermore, turbulence increases with higher molten Al fluidity at elevated pouring temperatures, though the effect is mitigated in VOC as mentioned earlier. Moreover, the increased fluidity also increases pouring velocity, leading to shorter pouring times, as shown in Table 3. The optimal pouring velocity was reported to be 50 cm/s and can be adjusted by modifying the pouring height [37]. In the present experiments, the recorded pouring velocity was 54.25 cm/s (Table 4), fixed by the pouring height as calculated in Equation 2. This velocity directly affects solidification, since higher pouring velocity (driven by either pouring height or fluidity) improves the ability of the molten Al to completely fill the mould before solidification occurs [37]. At low pouring temperatures — 800 °C for both orientations and 850 °C for the vertical casting — incomplete mould filling is evident in Figures 8a, 9a, and 9b, respectively. It has also been reported that casting porosity depends more strongly on pouring velocity than on pouring temperature itself [39].

This is evidenced by the decreased BP from an average of 13.04% at 800 °C to 3.24% at 900 °C, as seen in Figure 14(b), which is associated with an increase in impact toughness from an average of 10.5 kJ/m² at 800 °C to 16 kJ/m² at 900 °C, as shown in Figure 10(a). The microhardness of VOC, on the other hand, increased from an average of 82.7 HV at 800 °C to 101.5 HV at 900 °C (Figure 11(a)). A higher toughness requires greater ductility and is often associated with lower hardness [38]. The microhardness has also been reported to depend on porosity distribution [39] and pore size [38]. This is evident in the lower microhardness of HOC as seen in Figure 11(a) with the increased AP (Figure 14(a)) and BP (Figure 14(b)) with respect to the pouring temperature. On the contrary, VOC has shown fluctuating AP (Figure 14(a)) and decreased BP (Figure 14(b)) alongside decreased microhardness. Nevertheless, overall, VOC had higher microhardness than HOC with much lower AP and decreased BP. The microhardness measured in this study is more closely related to AP, since hardness testing reflects surface properties. As per cavity position, the middle cavity castings (positions 2 and 3) showed higher impact toughness as illustrated in Figure 10(b), with values of 13 kJ/m² and 16 kJ/m² for VOC and 6.67 kJ/m² and 7 kJ/m² for HOC, respectively. These correspond to lower microhardness values in Figure 11(b), presenting 90.6 HV and 95.27 HV for VOC and 88.87 HV and 91.63 HV for HOC, respectively. Again, the higher impact toughness and microhardness of VOC compared with HOC per cavity position correspond to lower AP in Figure 14(c) and BP in Figure 14(d).

The casting mass for the vertical orientation mould (252.4 g) and horizontal orientation mould (208.7 g) were calculated based on the density of 356 Al alloy of 2.68 g/cm³. The casting yield measures the weight of the castings in the cavities over the total poured casting, where the total mass of the four cast specimens was 76 g, the total casting mass for the vertical orientation mould was 252.4 g, and for the horizontal orientation mould was 208.7 g, as mentioned earlier.

The improvement in impact toughness associated with surface microhardness can be primarily attributed to the reduction in porosity within the castings, the AP, and the BP. A lower porosity decreases the number of internal defects and therefore the internal stresses, which enhances resistance to crack initiation and propagation under impact loading [40]. Furthermore, the improved impact toughness and microhardness properties of VOC, especially at elevated pouring temperatures and at middle cavity positions, are attributed to the vertical mould configuration as discussed earlier. Although the change in microhardness was relatively small (approximately 6% higher in VOC compared to HOC, with a maximum decrease of 18%), the impact toughness showed a more pronounced improvement, reaching up to 34% in VOC compared to only 8% in HOC. Although VOC showed a lower casting yield of approximately 30.11% compared to 36.40% for HOC, it achieved superior mechanical properties. Nevertheless, further investigation is required to address the influence of microstructural factors, such as cooling rate and phase distribution. In addition, numerical simulation of the pouring process may provide deeper insight into the relationship between melt flow behaviour and the resulting mechanical properties of the castings.

4. Conclusions

GDC moulds fabricated from ASTM A36 mild steel were arranged in vertical and horizontal orientations to produce 356 Al alloy castings at pouring temperatures of 800 °C, 850 °C, and 900 °C. Each casting contained four cavity positions,

which were evaluated for mechanical properties (Izod impact testing and Vickers microhardness) and physical characteristics (porosity testing). The following conclusions were drawn:

- HOC exhibited shorter pouring times but produced greater side flash at elevated pouring temperatures, particularly at 900 °C, whereas VOC showed casting misruns at 800 °C, mainly in distant cavity positions.
- Theoretical pouring times calculated using Torricelli's theorem were significantly lower than experimentally measured values, indicating the limited applicability of Torricelli's theorem for 356 Al alloy GDC under the present conditions. Furthermore, the gating system employed did not conform to the recommended minimum 10% expansion toward the casting.
- VOC demonstrated higher impact toughness, especially at middle cavity positions (positions 2 and 3), with a maximum value of 16 kJ/m², and toughness increased with pouring temperature, reaching the highest average at 900°C.
- Surface microhardness generally decreased with increasing pouring temperature, however, the maximum decrease was only 18% at VOC and only 6% higher than HOC overall.
- HOC exhibited significantly higher macro-porosity with large pores at elevated pouring temperatures, and BP and AP, particularly at elevated temperatures and distant positions, exhibiting higher porosity of 83% in AP and 24.3% in BP compared with VOC.
- VOC demonstrated superior overall casting performance at higher pouring temperatures, particularly at 900 °C, due to the vertical mould configuration, which incorporates open risers connected to each cavity, providing feeding of molten Al to the casting, minimising entrapped gases, and reducing solidification time.
- VOC produced a lower casting yield of 30.11% compared to 36.4% for HOC; however, VOC achieved superior mechanical properties, indicating a trade-off between yield efficiency and casting quality.
- Reductions in bulk porosity were directly associated with improvements in impact toughness in VOC, where BP decreased from 13.04% at 800 °C to 3.24% at 900 °C, corresponding to an increase in average impact toughness from 10.5 kJ/m² to 16 kJ/m². Surface microhardness showed a closer correlation with apparent porosity, with VOC consistently surpassing HOC in both microhardness and apparent porosity at all pouring temperatures.

The limitations of this work include the manual measurement of pouring time and controlling the mould preheating temperature. Future work may involve employing computational fluid dynamics (CFD)-based casting simulations to model the gravity die casting process and analyse melt turbulence, filling behaviour, and solidification characteristics under different casting orientations. The simulation results could then be validated against the experimental findings, and microstructural analysis could be employed to further investigate the relationship between flow behaviour, porosity formation, and mechanical properties.

Acknowledgements
The authors would like to thank Mr. Chang Weng Keong, owner of Mitsu Precision, Ipoh, Malaysia, for his generous support and assistance. The authors also gratefully acknowledge the financial support provided by Centre of Graduate Studies (CGS) at Universiti Tun Hussein Onn Malaysia (UTHM) through its postgraduate research funding scheme. Sincere appreciation is extended to the technicians of the Foundry Laboratory, Department of Mechanical Engineering Technology at UTHM for their technical assistance and provision of materials throughout this work.

Declaration of Competing Interests
The authors declare no conflicts of interest

CRediT Author Contribution Statement
Saleh Suliman Saleh Elfallah: Methodology, Investigation, Formal analysis, Data curation, Validation, Writing – original draft
Mohd Radzi Mohamed Yunus: Conceptualization, Supervision

Generative Artificial Intelligence Disclosure
The authors claim that artificially intelligent-assisted technologies, such as generative AI, were not used to generate content, ideas, or theories. The authors just utilised AI to enhance readability and refine the language. This was used with extreme human control and oversight. The authors take full responsibility for reviewing and approving the content.

References

[1] V.K. Lagisetti, C. Sukjamsri, "Machinability study on AA6061/2 SiC/graphite hybrid nanocomposites fabricated through ultrasonic-assisted stir casting," *International Journal of Automotive and Mechanical Engineering*, vol. 19, pp. 9950-9963, 2022. https://doi.org/10.15282/IJAME.19.3.2022.07.0767

[2] S.C. Tham, M.K. Sued, M.S. Salleh, N.I. Hussein, A. S. Anuar, M. M. Abdulatef, et al., "Cooling slope-cast LM25 aluminum fabrication for additive friction stir deposition: A microstructural and mechanical study," *International Journal of Automotive and Mechanical Engineering*, vol. 22, pp. 13002-13018, 2025. https://doi.org/10.15282/IJAME.22.4.2025.12.0989

[3] A. Patarić, M. Djurdjevic, S. Manasijevic, S. Stopic, M. Mihailović, "The role of silicon during solidification process of cast Al-Si-Mg alloys," *Materials*, vol. 18, no. 21, p. 5033, 2025. https://doi.org/10.3390/ma18215033

[4] Q. Cai, C. L. Mendis, I. T. Chang, Z. Fan, "Microstructure evolution and mechanical properties of new die-cast Al–Si–Mg–Mn alloys," *Materials & Design*, vol. 187, p. 108394, 2020.
[5] H. J. Kang, H. S. Jang, S. H. Oh, P. H. Yoon, G. H. Lee, et al., "Effects of solution treatment temperature and time on the porosities and mechanical properties of vacuum die-casted and T6 heat-treated Al–Si–Mg alloy," *Vacuum*, vol. 193, p. 110536, 2021. https://doi.org/10.1016/J.VACUUM.2021.110536
[6] L. Gao, Q. Wang, Q. Yang, W. Liu, B. Jiang, Y. Qin, et al., "Research on the mechanical properties and microstructural evolution of Al-Si alloy for automotive rear floors based on simulation-assisted casting," *Materials*, vol. 18, p. 2143, 2025. https://doi.org/10.3390/MA18092143/S1
[7] S. Zhao, L. Li, C. Li, Q. Han, L. Chen, L. Zuo, et al., "Influence of mg on microstructure and mechanical properties in al-mg-si alloy by gravity die casting," in *International Conference on Mechanical Manufacturing Technology and Material Engineering*, Singapore, 2024, pp. 455-461.
[8] F. M. M. Monteiro, "Development of the low pressure die casting and gravity sand casting processes for an Al steering knuckle," M.S. Thesis, University of Porto, Portugal, 2024.
[9] Z. Huda, "Die-casting processes," in *Metal Casting Engineering: Design, Processes, Calculations*, Switzerland: Springer Nature, 2025, pp. 199-218.
[10] M. Ceschini, G. Morri, F. Rotundo, and A. Toschi, "Heat treatment analysis and mechanical characterization of a recycled gravity die cast EN 42000 alloy," *Metals*, vol. 15, no. 7, p. 726, 2025. https://doi.org/10.3390/MET15070726
[11] V. Deev, E. Prusov, E. Ri, O. Prihodko, S. Smetanyuk, X. Chen, et al., "Effect of melt overheating on structure and mechanical properties of Al–Mg–Si cast alloy," *Metals*, vol. 11, no. 9, p. 1353, 2021.
[12] M. C. Mehta, D. Mandal, S. K. Chaudhury, "Microstructural changes and quality improvement of Al7Si0.2Mg (356) alloy by die vibration," *International Journal of Metalcasting*, vol. 14, no. 4, pp. 987–998, 2020. https://doi.org/10.1007/S40962-020-00408-3
[13] H. W. Doty, E. Samuel, A. M. Samuel, V. Songmene, F. H. Samuel, "Effect of melt treatment and heat treatment on the performance of aluminium cylinder heads," *Materials*, vol. 18, no. 5, p. 1024, 2025. https://doi.org/10.3390/MA18051024
[14] A. Samuel,Y. Zedan, H. Doty, V. Songmene, F. H. Samuel, "A review study on the main sources of porosity in Al-Si cast alloys," *Advances in Materials Science and Engineering*, vol. 2021, pp. 1921603, 2021.
[15] A. Akhyar, P. T. Iswanto, V. Malau, "Impact of pouring temperature on the mechanical properties of Al5.9Cu1.9Mg alloy," *Archives of Materials Science and Engineering*, vol. 113, no. 2, pp. 49–55, 2022. https://doi.org/10.5604/01.3001.0015.7016
[16] M. Syahid, L. H. Arma, H. Arsyad, Z. A. Suwardi, "Effect of pouring temperature on mechanical properties and microstructures of Al matrix composite strengthened by CNT with stir casting method," *Materials Science Forum*, vol. 988, pp. 30–35, 2020. https://doi.org/10.4028/www.scientific.net/msf.988.30
[17] C. Rajaravi, B. Gobalakrishnan, P. R. Lakshminarayanan, "Effect of pouring temperature on cast Al/SiCp and Al/TiB_2 metal matrix composites," *Journal of the Mechanical Behavior of Materials*, vol. 28, no. 1, pp. 162–168, 2019. https://doi.org/10.1515/jmbm-2019-0018
[18] M. Patel, S. K. Sahu, M. K. Singh, "Mechanical, tribological and corrosion behaviour of aluminium alloys and particulate reinforced aluminium or aluminium alloy metal matrix composites-A review," *i-Manager's Journal on Materials Science*, vol. 8, no. 2, p. 40, 2020. https://doi.org/10.5281/zenodo.5735521
[19] K. A. Gül, H. Sahin, and D. Dispinar, "Assessment of mechanical behaviors of sand cast Al-Mg7-Cu2 aluminum alloy in tilt and vertical gravity casting conditions," *Archives of Foundry Engineering*, vol. 25, pp. 169-79, 2025. https://doi.org/10.24425/afe.2025.153787
[20] D. Du, J. An, A. Dong, B. Sun, "A review of the progress and challenges of counter-gravity casting," *Journal of Materials Science & Technology*, vol. 1, pp. 1-26, 2025. https://doi.org/10.1016/j.jmst.2024.07.037
[21] ASTM A36/A36M-19, Standard Specification for Carbon Structural Steel, ASTM International, West Conshohocken, PA, USA, 2019.
[22] ASTM B108/B108M, Standard Specification for Aluminium-Alloy Permanent Mold Castings, ASTM International, West Conshohocken, PA, USA, 2025.
[23] R. Bahador, N. Hosseinabadi, A. Yaghtin, "Microstructural and mechanical characterizations of stir cast aluminium 356–Nb_2O_5 composite," *Advanced Composites and Hybrid Materials*, vol. 3, no. 4, pp. 594–608, 2020. https://doi.org/10.1007/s42114-020-00173-1
[24] J. Campbell, *Complete casting handbook*, 2nd ed. Oxford, U.K.: Butterworth-Heinemann, 2015.
[25] V. Kumar, J. Madan, P. Gupta, "A system for design of multiposition die casting dies from part product model," *The International Journal of Advanced Manufacturing Technology*, vol. 67, pp. 2083–2107, 2013. https://doi.org/10.1007/s00170-012-4633-y
[26] H. Pratikno, A. H. Baredwan, W. L. Dhanista, "Effect of preheating process and V groove type on the tensile and metallography test of ASTM A53 with A36 weld joint using FCAW method," *International Journal of Offshore and Coastal Engineering*, vol. 6, no. 2, pp. 40–45, 2021.
[27] M. Neuser, O. Grydin, Y. Frolov, M. Schaper, "Influence of solidification rates and heat treatment on the mechanical performance and joinability of the cast aluminium alloy AlSi10Mg," *Production Engineering*, vol. 16, no. 2, pp. 193-202, 2022. https://doi.org/10.1007/s11740-022-01106-1

[28] A. M. Samuel, E. Samuel, V. Songmene, F. H. Samuel, "A review on porosity formation in aluminum-based alloys," Materials, vol. 16, no. 5, p. 2047, 2023. https://doi.org/10.3390/ma16052047
[29] AWS D1.1/D1.1M:2015, *Structural welding code – steel*, American Welding Society, Miami, FL, USA, 2015.
[30] D. Alvaro-Berlanga, R. Planet, A. Fernández-Nieves, "Torricelli's experiment and conservation of momentum," *American Journal of Physics*, vol. 92, no. 7, pp. 493–497, 2024. https://doi.org/10.1119/5.0145991
[31] P. Futas, A. Pribulova, V. Sabik, J. Petrik, P. Blasko, M. Brzeziński, "Elimination of shrinkage in ductile iron castings using computer simulation of casting and solidification," *Processes*, vol. 12, no. 3, p. 506, 2024. https://doi.org/10.3390/pr12030506
[32] M. Durmuş, D. Dispinar, M. Gavgali, E. Uslu, M. Çolak, "Evaluation of Fe content on the fluidity of 356 Al alloy by new fluidity index," *International Journal of Metalcasting*, vol. 19, no. 3, pp. 1590–1604, 2025. https://doi.org/10.1007/s40962-024-01396-4
[33] G. W. Stachowiak, A. W. Batchelor, *Engineering tribology*, 4th ed. Oxford: Butterworth-Heinemann, 2014.
[34] B. Jiang et al., "Study on the influence of injection velocity on the evolution of hole defects in die-cast aluminum alloy," *Materials*, vol. 17, no. 20, p. 4990, 2024. https://doi.org/10.3390/ma17204990
[35] C. Thongyothee and S. Chareonvilisiri, "The effect of gas venting on the mechanical properties of C95800 aluminum bronze castings," *Engineering, Technology & Applied Science Research*, vol. 15, no. 4, pp. 25068–25075, 2025. https://doi.org/10.48084/etasr.10993
[36] Y. Xiao, C. Xiao, D. Chang, Y. Ji, B. Wang, F. Li, et al., "Time-varying disturbances of temperature field in investment casting and corresponding shrinkage defects control methods," *Journal of Materials Research and Technology*, vol. 35, pp. 5147-5159, 2025. https://doi.org/10.1016/j.jmrt.2025.02.164
[37] S. Chakravart and S. Sen, "An investigation on the solidification and porosity prediction in Al casting process," Journal of Engineering and Applied Science, vol. 70, no. 21, 2023. https://doi.org/10.1186/s44147-023-00190-z
[38] M. T. Di Giovanni, J. T. de Menezes, E. Cerri, E. M. Castrodeza, "Influence of microstructure and porosity on the fracture toughness of Al–Si–Mg alloy," *Journal of Materials Research and Technology*, vol. 9, no. 2, pp. 1286–1295, 2020. https://doi.org/10.1016/j.jmrt.2019.11.055
[39] W. Li, A. Amanov, K. M. Nagaraja, B. Li, B. B. Ravichander, R. Zhang, et al., "Processing aluminium alloy with hybrid wire arc additive manufacturing and ultrasonic nanocrystalline surface modification to improve porosity, surface finish, and hardness," *Journal of Manufacturing Processes*, vol. 103, pp. 181–192, 2023. https://doi.org/10.1016/j.jmapro.2023.08.047
[40] H. Xie, Y. Li, J. Song, L. Qin, H. Hu, C. Li, et al., "Mechanism of pore-induced damage evolution and failure in high pressure die casting Ae81 magnesium alloy: An in-situ sem and micro-Ct study, " *Journal of Alloys and Compounds*, vol. 1030, p. 180903, 2025. https://doi.org/10.1016/j.jallcom.2025.180790